



ELSEVIER

Contents lists available at ScienceDirect

Structures

journal homepage: www.elsevier.com/locate/structures

Experimental investigation of the residual behaviour of damaged masonry arch structures

L. Augusthus-Nelson^{a,*}, G. Swift^{b,*}^a School of Science, Engineering and Environment, University of Salford, Salford M5 4WT, United Kingdom^b School of Earth & Environmental Science, University of Portsmouth, Portsmouth PO1 2UP, United Kingdom

ARTICLE INFO

Keywords:

Masonry arch bridge
Physical modelling
Residual strength
Cyclic loading
Quasi-static loading
Serviceability and permissible limit states
Reliability of masonry arch structures

ABSTRACT

New masonry arch bridges are rarely constructed as part of modern transport networks, however they continue to remain an integral part of modern civil infrastructure due to their overall resilience. This resilience has led to extremely long service lives which in turn has led to the majority of those bridges still in service being either distorted or damaged. Interest in the bridge owners community is directed towards prolonging the service life of these structures rather than replacement with new bridges. The aim of this paper is to explore whether the residual strength and the service life can be reliably established, and whether load limits must be imposed based on condition-based assessment, and/or retrofit the masonry arch system to prolong the life span of these important structures.

To investigate residual strength and safe working loads, large scale, soil-backfilled masonry arches were constructed and subsequently subjected to a range of loading scenarios in controlled laboratory environments. Post-failure, these structures were further tested using both cyclic and quasi-static loadings. Results shows that: repeated cyclic loading at safe working load levels do not significantly alter the ultimate load carrying capacity of virgin masonry arch structures; the residual strength of distorted and/or damaged arch structures can be significant; distorted and/or damaged bridges are to some extent able to heal when subjected to repeated cyclic loading at safe working load levels, which is not the case with a virgin arch. Based on these findings, it can be concluded that the safe working load and life span of distorted and/or damaged masonry arch structures must be established in conjunction with the current state of the masonry arch structure.

1. Introduction

It has long been recognised that masonry arch bridges form an integral component of the transport network in the United Kingdom (UK), with Page et al. [23] identifying 40,000 such structures, representing about 40% of the bridge stock. The problem extends far beyond the UK though, with many examples found across Europe [9,15,21] and the United States [5], and beyond. Gilbert et al. [12] suggest that there are approximately one million masonry arch bridge spans currently in service around the world. In addition to their widespread use, is the issue of their longevity; their age and condition. Orban and Gutermann [22] states that more than 60% of the masonry arch structures in use across the European rail network are in excess of 100 years old, with the majority in the UK alone in excess of 120 years old. This is clearly an issue, one that has been recognised for some time, with increasing concerns raised about the reliability of these long-lived structures and an awareness of the need for appropriate modelling and assessment methodologies (for example, [19,12]).

Replacement is one option, but often discounted due to the expense, but also due to the importance of these structures to our architectural and cultural heritage; as McKibbins et al. [19] observe, these structures might be viewed as among the most sustainable ever to have been built. Instead, remediation and repair tend to be the progressive options, based around some form of load capacity and structural assessment.

Although there have been significant advances in the analytical tools that can be applied to masonry arch structures (eg. [7,20,10]), as well as improved methods of monitoring (eg. [27,1]), allowing large volumes of data to be collected and analysed, there has been little work done to inform the development of decision support tools; although tools exist, these are simplified and are not capable of identifying bridges which are vulnerable to load induced deterioration.

Throughout Europe assessment methods generally fall into three categories identified by [14,17,19]: the semi-empirical MEXE method (including a number of modified versions); elastic analysis methods with limits set on the stress levels; and ultimate limit state methods

* Corresponding authors.

E-mail addresses: l.augusthusnelson@salford.ac.uk (L. Augusthus-Nelson), gareth.swift@port.ac.uk (G. Swift).<https://doi.org/10.1016/j.istruc.2020.08.008>

Received 4 November 2019; Received in revised form 10 March 2020; Accepted 3 August 2020

2352-0124/© 2020 The Author(s). Published by Elsevier Ltd on behalf of Institution of Structural Engineers. This is an open access article under the CC BY license (<http://creativecommons.org/licenses/by/4.0/>).

based upon a ‘mechanism’ approach or a non-linear FE analysis (eg. [8,20,11]). The residual capacity of the arch bridge is not explicitly considered by any of these approaches, yet with growing financial pressures on bridge owners, the residual life of a bridge is an area that is of paramount importance that could be used to prioritise conflicting maintenance demands on limited budgets.

To date little work has been undertaken on damaged masonry arch structures subjected to ‘real-world’ loading conditions. In light of this, carefully controlled experimental work has been carried out to examine the behaviour and residual capacity of damaged, full-scale, backfilled masonry arches. This experimental work forms part of a wider programme of research aimed at examining the relationship between the ultimate limit state (ULS), defined here as the condition at which a collapse mechanism forms in the structure or its supports, and the permissible limit state (PLS) as defined by Melbourne et al. [17] as the limit at which there is a loss of structural integrity that will measurably affect the ability of the bridge to carry its working loads for the expected life of the bridge. Specifically, the paper aims to consider the limiting PLS criteria to make this assessment possible.

It is anticipated that the results from these full-scale tests on virgin and distorted/damaged arches could provide experimental evidence to calibrate computational and semi-empirical models and could therefore provide useful insight to inform the assessment process.

This paper describes a series of large-scale laboratory tests investigating the behaviour of damaged masonry arch bridges. The experimental arrangement is described in detail, before test results are presented and discussed in the context of possible real-world application.

2. Experimental methodology

All tests were carried out on near identical 3 m span brickwork arches constructed and backfilled with either clay or crushed limestone in a purpose made test chamber, the detailed design and construction of which is described elsewhere [6,25,4,3]. In all cases, the virgin arch barrel has a segmental radius of 1.875 m and a span of 3 m, with a nominal span to rise ratio of 4:1. The arch barrel consists of two rings and alternate courses containing headers, used to eliminate the issues arising from ring separation problems. Fig. 1 shows the general arch geometry, whilst Fig. 2 shows schematically the arch barrel and backfill within the test chamber, as well as the loading arrangement.

In three of the tests reported, the backfill employed was a compacted, crushed limestone (EP1, EP2 and EP5); in the fourth test (EP4) a clay backfill material was used. In all tests the backfill was placed to a depth of 300 mm above the arch crown.

The limestone backfill used in the tests is commonly employed in practice, and is a graded crushed limestone. This material was compacted in 120 mm thick layers in a carefully controlled manner to achieve an average as-placed unit density of 2.0 Mg/m³. The clay fill was placed using a similar methodology as with the limestone, however, the material was conditioned by varying the as-delivered moisture

content in accordance with the optimum moisture content as determined from laboratory compaction tests, prior to placement. Properties of the limestone and clay are shown in Table 1.

The loading arrangement, as shown in Fig. 2, was designed to simulate highway loading conditions and sufficiently adaptable to allow application of both cyclic loading, representing working loading conditions in an in-service bridge, and quasi-static loading, allowing determination of bridge load carrying capacity.

The mechanical and hydraulic systems and the associated control system used in these tests are described in detail in Augustus-Nelson et al. [4,3]. However, in essence five no. servo-controlled hydraulic actuators, with a maximum load capacity of 200 kN were used to apply a ‘line’ cyclic or quasi-static load to the level surface of the soil backfill above the springing, quarter spans and crown of the arch barrel, depending on the test being undertaken (Fig. 2). Each arch was subjected to a range of loading regimes which are specified in Table 2. In order to quantify the stiffness of the arch, a slower rate (0.01 Hz) of cyclic loading was applied at various stages. This period of slow loading also allowed images to be collected for subsequent Particle Image Velocimetry (PIV) analysis, allowing kinematic observations to be made and potential validation for numerical analyses.

In all tests reported on herein, the first phase and stage involved de-centering, involving the removal of the steel support used during the brick arch construction, allowing unrestrained deformation of the arch barrel during subsequent load testing. A number of subsequent test phases and stages were then implemented, as described in the next paragraphs.

In EP1, the first phase involved a period of cyclic loading using all five actuators in sequence, at 2 Hz with a peak load of 50 kN for 10⁶ cycles. This frequency of loading was consistent with previous arch tests conducted by, for example, Melbourne & Alnuaimi [16], and simulates vehicle passage whilst avoiding dynamic inertial effects. This pattern of loading was also used in the first phase of EP4, allowing a direct comparison between two arches subjected to near-identical working loading conditions, but with different backfill material: coarse-grained fill in the case of EP1, and a fine-grained fill in the case of EP4.

Once this stage was complete, the arch was then subjected to a quasi-static load test to failure (QS1) using the actuator located directly over the quarter-span of the barrel. Once failure had been observed, the second phase of this test required the careful re-setting of the arch barrel (RA1). The intention here was to attempt to restore the arch profile to as close to its original form as was practicable, through the application of backfill surface loads. In most cases all five loading beams were used and placed on the backfill surface at positions consistent with those used for the cyclic load regime, and a quasi-static load of 50 kN was applied sequentially at each position from the western abutment to the eastern abutment, in order to push the arch barrel towards its original profile. The resetting procedure allowed only a proportion of the original distortion to be restored; the degree of permanent deformation would vary between tests. This means that the initial profile of the arch at the beginning of a given phase of loading

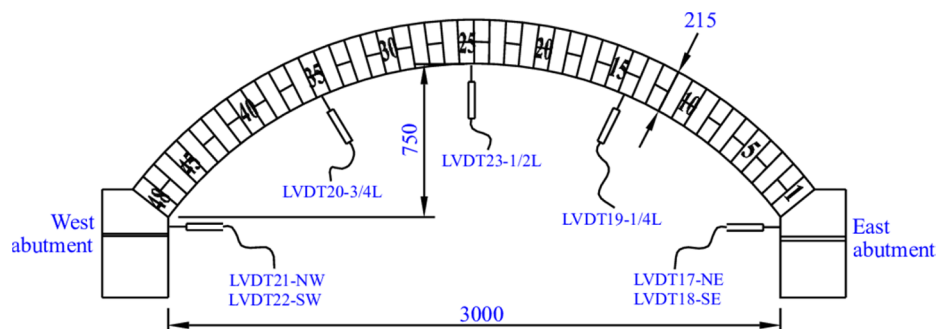


Fig. 1. General arrangement of the arch barrel and abutments, with the location of the displacement transducers (after [2]).

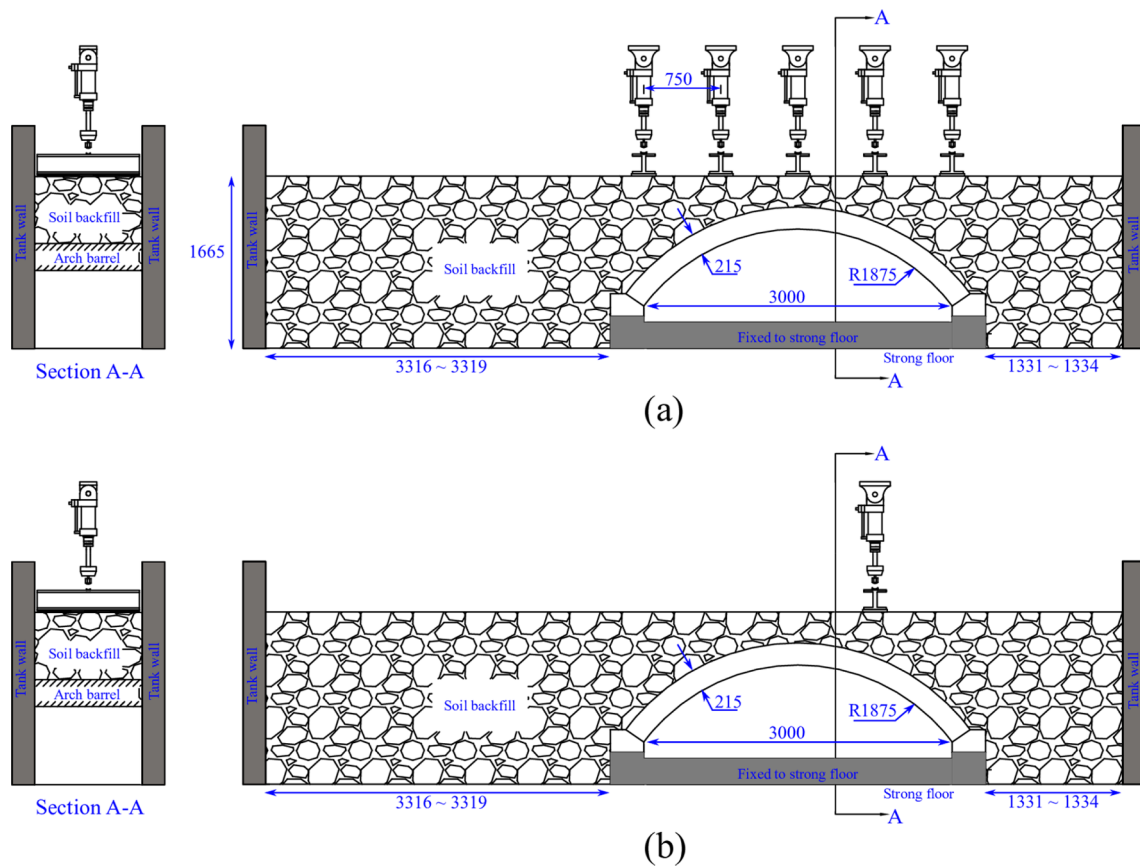


Fig. 2. Location of arch barrel related to test chamber and loading arrangements of (a) cyclic loading and (b) quasi-static failure load test.

Table 1
Backfill properties.

Limestone	
Unit weight	20 kN/m ³
Drained shear strength	$c' = 3.3 \text{ kN/m}^2; \phi' = 54.5^\circ$
Clay	
Liquid limit	37%
Plastic limit	14%
Passing 425 μm	98%
Optimum moisture content	14%
Maximum unit dry density	1.9 Mg/m ³
As-placed moisture content	18.2%

differed from the corresponding profile in the preceding phase. The distorted profiles will be considered in more detail later in this paper.

Once the arch barrel shape had been re-established, a second stage of cyclic loading was undertaken, again, using all five actuators in series at a load rate of 2 Hz and maximum load of 50 kN for 10⁵ cycles. At the end of this stage, the damaged arch capacity was investigated through a second quasi-static load test to failure (QS2).

The arch test for EP2 was identical to EP1 with the omission of the cyclic loading regimes before and after the first quasi-static loading regime, allowing a direct comparison between an arch subject to predominantly real-world loading conditions, and a virgin arch barrel. EP4 involved the same test stages as EP1, however, additional quasi-static load tests were conducted on this structure (3no. in total: QS3), followed by a range of cyclic load tests to explore the permissible limit state as defined by Melbourne et al. [18] and Gilbert et al. [12]. However, to establish the permissible limit state of a virgin arch bridge, which is not subjected to any quasi-static load test, EP5 involved a

larger number of cyclic loading stages (5no.), subsequently followed by a quasi-static load test to failure.

The cyclic loading regimes described above specify a peak load of 50 kN. The selection of this live load level to apply to the test structures was based on a consideration of the expected ULS informed by experimental evidence from previous test programmes, combined with an appropriate ‘global’ factor of safety to define a level of service loading that could safely be applied to the arch barrel. This represents a measure of the Serviceability Limit State (SLS), defined in terms of a factor of safety of 2 on an anticipated failure load (ULS) of between 100 and 150 kN, based on previous experience of testing backfilled brick arches of this type. This is consistent with current arch bridge assessment documents, particularly those in the UK, which simply indicate that it will be prudent to limit the regularly applied loads to half the ultimate failure load [26]. A value towards the lower bound of the range quoted was selected to minimise risk of accumulated damage to the arch barrel during cyclic loading.

It is recognised that the resulting limit on the live load could prove over-conservative, and this is discussed later. However, within the experimental data presented, some attempt has been made to examine this issue in more detail, with particular reference to the PLS.

As the main focus of this paper is the residual behaviour of damaged arch structures in particular, there are inevitably some aspects of these tests that will not be considered in detail.

3. Experimental results and discussion

A fundamental question driving the testing programme was: to what degree does in-service or working loads influence the carrying capacity of a masonry arch, whether this is a virgin arch structure, or one that has suffered some form of structural damage? The results of virgin and distorted/damaged arches have been discussed separately for this

Table 2
Test sequences of EP1, EP2, EP4 and EP5.

Test Phase	Test Stage	Peak Load	Number of cycles	Frequency/loading rate	Notes
EP1 – Limestone backfilled arch					
PH1	CYC1	50 kN	10 ⁶ cycles	2 Hz	Faster cyclic loading test
	CYC2	50 kN	6 cycles	0.01 Hz	At the start, after 10 ⁴ , 10 ⁵ and 10 ⁶ cycles during faster cyclic loading test
	QS1	Load to failure	–	–	Manual displacement control test
PH2	RA1	50 kN	1 cycle	0.01 Hz	Arch resetting procedure
	CYC1	50 kN	10 ⁶ cycles	2 Hz	Combination of faster and slower cyclic loadings
	QS2	Load to failure	–	–	Manual displacement control test
EP2 – Limestone backfilled arch					
PH1	QS1	Load to failure	–	10 mm/hr	Automated displacement control test
PH2	RA1	50 kN	1 cycle	<0.01 Hz	Arch resetting procedure
	QS2	Load to failure	–	10 mm/hr	Automated displacement control test
EP4 – Clay backfilled arch					
PH1	CYC1	50 kN	10 ⁶ cycles	2 Hz	Faster cyclic loading test
	CYC2	50 kN	6 cycles	0.01 Hz	At the start, after 10 ⁴ , 10 ⁵ and 10 ⁶ cycles during faster cyclic loading test (PH1-CYC1)
	QS1	Load to failure	–	10 mm/hr	Automated displacement control test
PH2	RA1	50 kN	1 cycle	<0.01 Hz	Arch resetting procedure
	CYC1	50 kN	10 ⁵ cycles	2 Hz	Faster cyclic loadings test
	CYC2	50 kN	6 cycles	0.01 Hz	At the start, after 10 ⁴ and 10 ⁵ cycles during faster cyclic loading test (PH2-CYC1)
	QS2	Load to failure	–	10 mm/hr	Automated displacement control test
PH3	RA1	50 kN	1 cycle	<0.01 Hz	Arch resetting procedure
	CYC1	50 kN	10 ⁵ cycles	2 Hz	Faster cyclic loadings test
	CYC2	50 kN	6 cycles	0.01 Hz	At the start, after 10 ⁴ and 10 ⁵ cycles during faster cyclic loading test (PH3-CYC1)
	QS2	Load to failure	–	10 mm/hr	Automated displacement control test
PH4	RA1	50 kN	1 cycle	<0.01 Hz	Arch resetting procedure
	CYC1	50 kN	10 ⁴ cycles	2 Hz	Faster cyclic loadings test
	CYC2	60 kN	10 ⁴ cycles	2 Hz	Faster cyclic loadings test
	CYC3	66 kN	10 ⁴ cycles	2 Hz	Faster cyclic loadings test
	CYC4	72 kN	10 ⁴ cycles	2 Hz	Faster cyclic loadings test
	CYC5	78 kN	10 ⁴ cycles	2 Hz	Faster cyclic loadings test
	CYC6	84 kN	10 ⁴ cycles	2 Hz	Faster cyclic loadings test
	CYC7	90 kN	<10 ⁴	2 Hz	Faster cyclic loadings test
	CYC8	50 kN	6 cycles	0.01 Hz	Slower cyclic loading test, between every CYCs in PH4
EP5 – Limestone backfilled arch					
PH1	CYC1	50 kN	10 ⁵ cycles	2 Hz	Faster cyclic loadings test
	CYC2	60 kN	10 ⁵ cycles	2 Hz	Faster cyclic loadings test
	CYC3	70 kN	10 ⁵ cycles	2 Hz	Faster cyclic loadings test
	CYC4	80 kN	10 ⁵ cycles	2 Hz	Faster cyclic loadings test
	CYC5	90 kN	10 ⁵ cycles	2 Hz	Faster cyclic loadings test
	CYC6	100 kN	<10 ⁵	2 Hz	Faster cyclic loadings test
	CYC8	50 kN	6 cycles	0.01 Hz	Slower cyclic loading test, between every CYCs in PH1
		QS1	Load to failure	–	10 mm/hr

Yellow QS (failure load) tests considered as a virgin arch - no deformation in the arch barrel.
Green QS (failure load) tests considered as distorted/damaged arch (deformed shape profile can be found in Table 3).

matter. As explained in the preceding section, there are differences in the cyclic loading regimes and the reader is advised to be mindful of this when inspecting the results.

3.1. Virgin arch

As mentioned earlier, all tests started with the de-centering process. It should be noted that the test arches were monitored during the de-centering process prior to any application of load, using the displacement transducers (Fig. 1). No significant movements were observed during this process. Therefore, it is assumed that the shape of the arch barrel at the start of each test was essentially identical.

3.1.1. Influence of cyclic loading (peak cyclic load below the serviceability limit)

EP1 and EP2 were constructed and backfilled in a near-identical manner with the same crushed limestone backfill. However, EP1 was subjected to a period of cyclic loadings, which consists of one million cycles of 2 Hz and 50 kN peak load (faster cyclic loading regime), and a

series of six cycles of 0.01 Hz and 50 kN peak load (slower cyclic loading regime) at the start, after 10⁴, 10⁵ and 10⁶ cycles of faster cyclic loadings (Fig. 3 and Table 2). It is recognised that this cyclic load level (peak load of 50 kN) is below what would be expected to be below the serviceability limit state for this structure, and possibly below the permissible limit load. The cyclic loading regimes used are presented in Fig. 3.

Arch barrel behaviour was observed throughout the cyclic loading tests of EP1. Arch barrel deformations during all the six cycle loading regimes (0.01 Hz and 50 kN peak load) prior to first quasi-static failure load test are illustrated in Fig. 4. The first slower cyclic loading test showed a slightly different behaviour to the rest of the slower rate cyclic loading tests, but the response in all cases indicated apparently elastic behaviour, i.e. recoverable, and at a very low level (< 0.7 mm peak displacement). In addition, during the first 10⁴ cycles of faster cyclic loading test, surface settlements directly beneath the loading beams were observed. The observations showed that there was no change in the profile of backfill for the remaining one million cycles.

The behaviour indicated in the first 10⁴ cycles may be attributed to

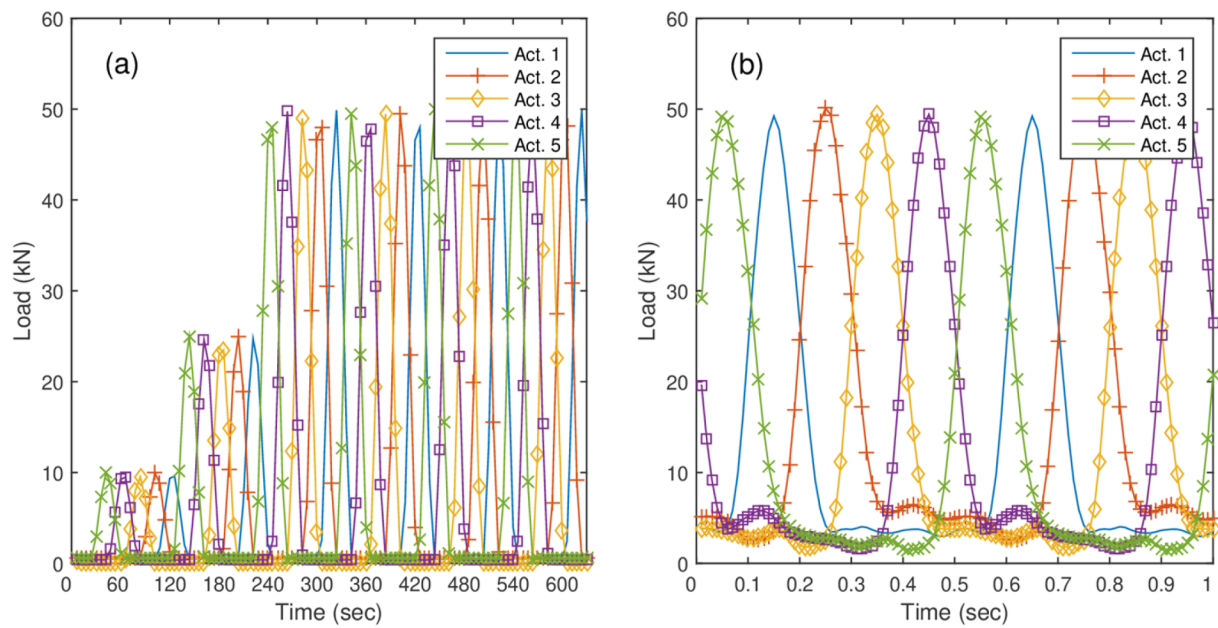


Fig. 3. (a) Entire slower cyclic loading regime (the same for all the tests) (b) faster cyclic loading regime (peak load was varied for part of EP4 and EP5) (after [2]).

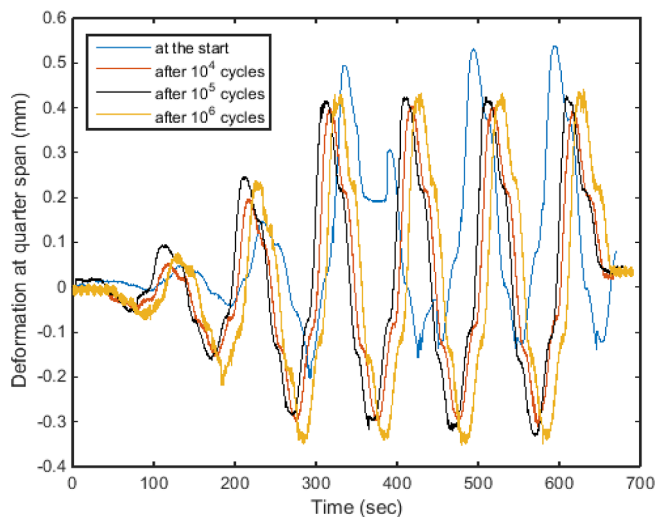


Fig. 4. Displacement against the time for the slower cyclic loading tests of EP1 prior to first quasi-static failure load test.

the construction stages of the arch bridge, where the soil is densified, and the arch may simply have repositioned itself to the most stable position. Thereafter, changes in the stiffness of the arch-backfill system are insignificant, as the near-constant amplitude indicates in Fig. 4. In addition, on inspection of the arch intrados, no cracks were evident in the arch barrel. It can be concluded that the cyclic loading below the safe working load may positively contribute to the system stability by increasing the stiffness of the backfilled masonry arch system. For subsequent discussions all of the arches subjected to one million cycles with peak load of 50 kN and with a frequency of 2 Hz were considered as a virgin arch.

3.1.2. Initial arch capacity and failure mechanism

Fig. 5 presents the load vs. deflection curves for the first quasi-static failure load test (QS1) for EP1, EP2 and EP4. EP1 and EP2 were subjected to a quasi-static load to induce failure and it is evident from this figure that the carrying capacity of the two arches is similar indicating that this period and level of cyclic loading had little impact on the arch carrying capacity, supporting the hypothesis that the level of cyclic

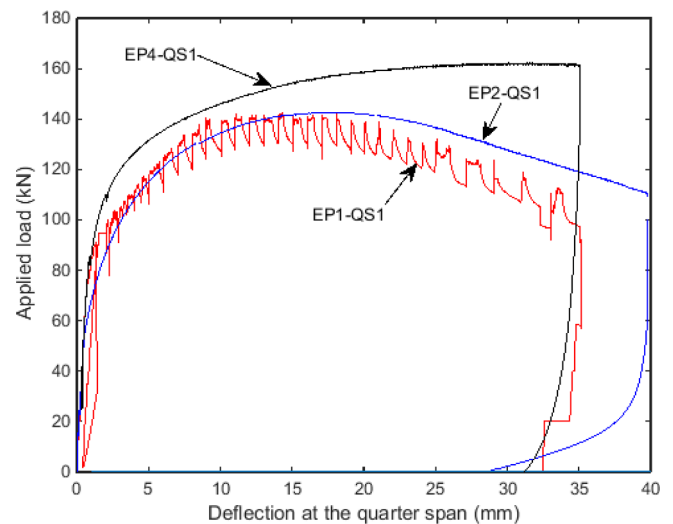


Fig. 5. First quasi-static failure load tests of EP1, EP2 and EP4.

loading (as described in Section 3.1.1) was both below the serviceability limit, but also suggesting that it may also be lower than the permissible limit state. Fig. 6(a) illustrates the failure mechanism for the two arches; in both cases, a four-hinge mechanism is evident. Fig. 7 shows corresponding GeoPIV plots generated from digital analysis conducted on images of the backfill and arch deformation during testing. This figure illustrates the kinematic response of the backfill to the load application and to the deforming arch barrel, and the data is consistent with observations made by Melbourne and Alnuaimi [16] and Page et al. [23], for instance. The applied load is dispersed through the fill, but this dispersal is within a relatively narrow zone, with the arch barrel moving away from the backfill (active). In contrast, the passive zone in which the arch barrel moves towards the backfill encompasses a much larger volume of fill material. Much of the movement is confined to the arch barrel in both cases, although the vectors do indicate some displacement adjacent to the abutments. Abutment movements were monitored during testing and were seen to be of the order of 5 mm and < 1 mm for the west and east abutments of EP1 and EP2, as shown in Fig. 8.

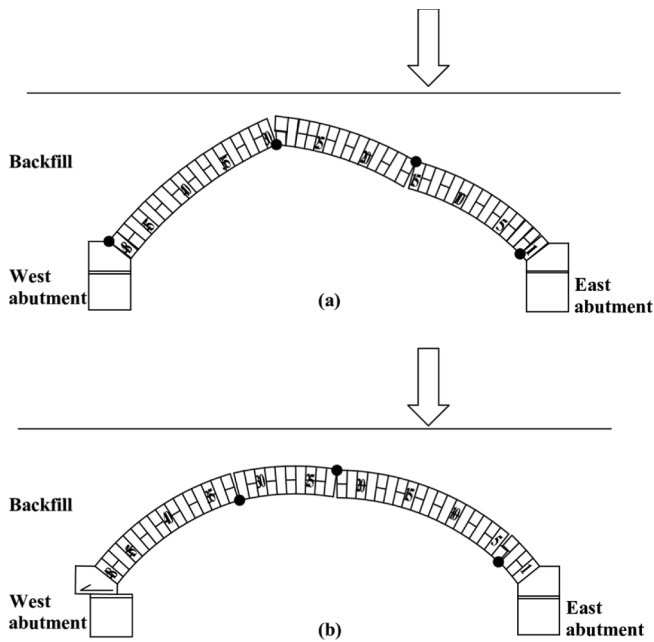


Fig. 6. Failure mechanism at first quasi-static load test of (a) EP1 and EP2 (b) EP4.

The main difference in results between EP1 and EP2 (Fig. 5) appear to relate to the initial stiffness of the arch-backfill system, as illustrated by the gradient of the corresponding load–deflection curves. This is likely attributable to densification of the soil backfill during cyclic loading during EP1, as described in Section 3.1.1.

During the EP1 quasi-static load test, an unload-reload loop occurred when the actuator load reached a level of around 90 kN (Fig. 5). Although not intentional, this provided some insight in to the behaviour

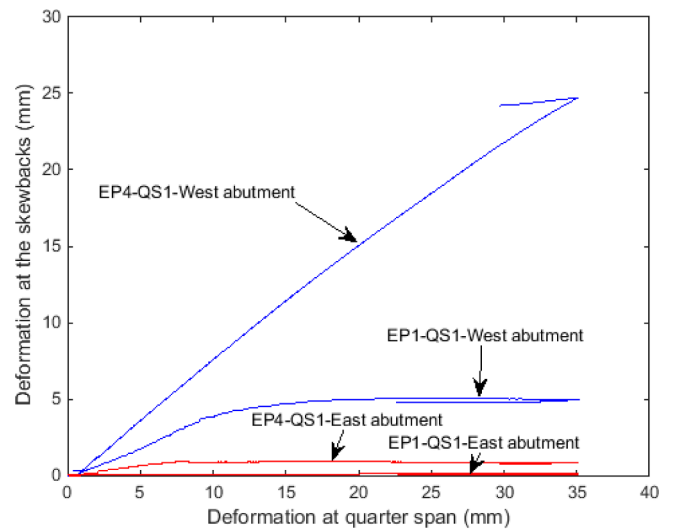


Fig. 8. Horizontal deformations of east and west abutments during first quasi-static failure load tests of EP1 and EP4.

of the system; in this case, there was no observable change in response of the system to this action, possibly suggesting that essentially elastic behaviour might be assumed up to loads consistent with this level, i.e. 90 kN.

The experimental data indicates that EP1 and EP2 achieved a similar peak load at approximately 140 kN, whereas EP4, comprising of a clay backfilled arch, achieved a peak of around 160 kN as illustrated in Fig. 5 (note that two more quasi-static load tests were carried out, which are not considered in this section). EP4 was also subjected to the same cyclic loading regimes as EP1. In the case of EP4, quite large deflections were required before full resistance was mobilised. The initial system stiffness was quite similar in all three tests, with EP2 and

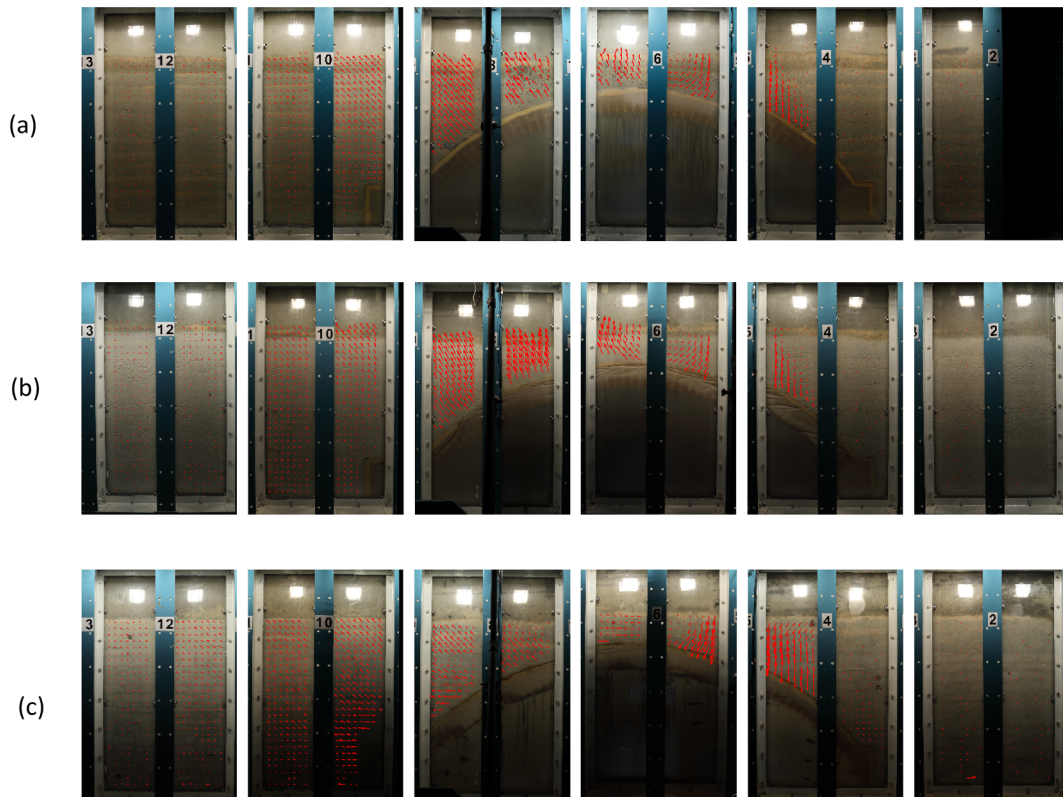


Fig. 7. Particle Image Velocimetry output from the start of the test until the maximum load (a) EP1_QS1 (b) EP2_QS1 (c) EP4_QS1.

EP4 showing similar stiffness profiles up to an applied load of around 60 kN, and EP1 and EP4 showing a similar stiffness profile up to around 80 kN. Figs. 6 and 7 also compare the difference in failure mechanisms and soil deformation, respectively. The western abutment slides outwards during the first quasi-static loading test of EP4 (Fig. 8), indicating that the overall failure was due to three hinges and sliding at the abutment, which was different from EP1 and EP2. Results indicated that the behaviour of the arch barrel and observed failure mechanisms were significantly influenced by the backfill materials.

3.1.3. Influence of cyclic loading above permissible load

As with EP1 and EP2, EP5 was constructed and backfilled in a near-identical manner with the same crushed limestone backfill, to investigate the effect of various peak cyclic loads and to investigate serviceability and permissible limit states.

At the start of EP5, the six cycle, slower cyclic loading regime (0.01 Hz and 50 kN peak load) was employed. This was followed by 10^5 cycles faster cyclic loading regime (2 Hz and with 50 kN peak load). These cyclic loading regimes were exactly the same as the cyclic loadings were applied to EP1. The results of EP1 and EP5 show that both arches exhibited similar behaviour. Hence, the expected failure load of EP5 may be taken as that of EP1 and EP2, which was 140 kN. Thereafter, the arch-backfill system was subjected to the same slower cyclic loading and then faster loading regime (2 Hz) with peak load of 60 kN. The loading sequences were continued, however, the peak load of the faster loading regime was increased by 10 kN until the peak load of 100 kN was reached, as illustrated in Fig. 9. Finally, the six cycle, slower cyclic loading regime was applied to compare the stiffness changes in the arch-backfill system.

Up to a peak load of 80 kN there was no significant changes in the arch barrel except the slip in the LVDT and slightly larger deformation amplitude in the radial direction compared to response at 70 kN, as expected (Fig. 9(a)). Soon after the start of the 90 kN level of cyclic loading, intrados bricks near the quarter span were displaced and subsequently lost from the main structure (Fig. 10), knocking an LVDT, which is identified in Fig. 9(a). However, the arch-backfill system was evidently able to accommodate the 90 kN cyclic load with only a small increase in the deformation amplitude. Similarly, at the beginning of the 100 kN cyclic load phase, displacement and loss of bricks was observed, as shown in Figs. 9(b), 10 and 11. Loss of bricks subsequently reduced the stiffness of the system significantly and the test was very dynamic due to large deformation in the arch barrel. A larger actuator stroke length was required in order to accommodate this magnitude of deformation, which ultimately was not possible due to the hydraulic pump capacity.

Fig. 12 compares the quarter span deformation during all the slower rate tests. The arch barrel was altered during the 90 kN peak cyclic loading regime. Changes in stiffness after 90 kN was not significant compared to the previous slower rate tests, however the stiffness of the arch after 100 kN was significantly lower compared to the slower cyclic loading below 100 kN.

3.1.4. Safe working load

The ultimate limit state of masonry arch bridges has a general agreement among most researchers and assessors. However, there are no agreed definitions for serviceability (SLS), fatigue (FLS) and durability (DLS) limit states. Previous research (eg, [16]) has attempted to quantify the load level at which no further deleterious effects in the arch is observed. This has developed towards identifying a PLS limit that could inform the Sustainable Masonry Arch Resistance Technique (SMART) method of arch assessment, based on the work of Melbourne et al. [17]. PLS is defined as the limit at which there is a loss of structural integrity that measurably affects the ability of the bridge to carry its working loads for the expected life of the bridge.

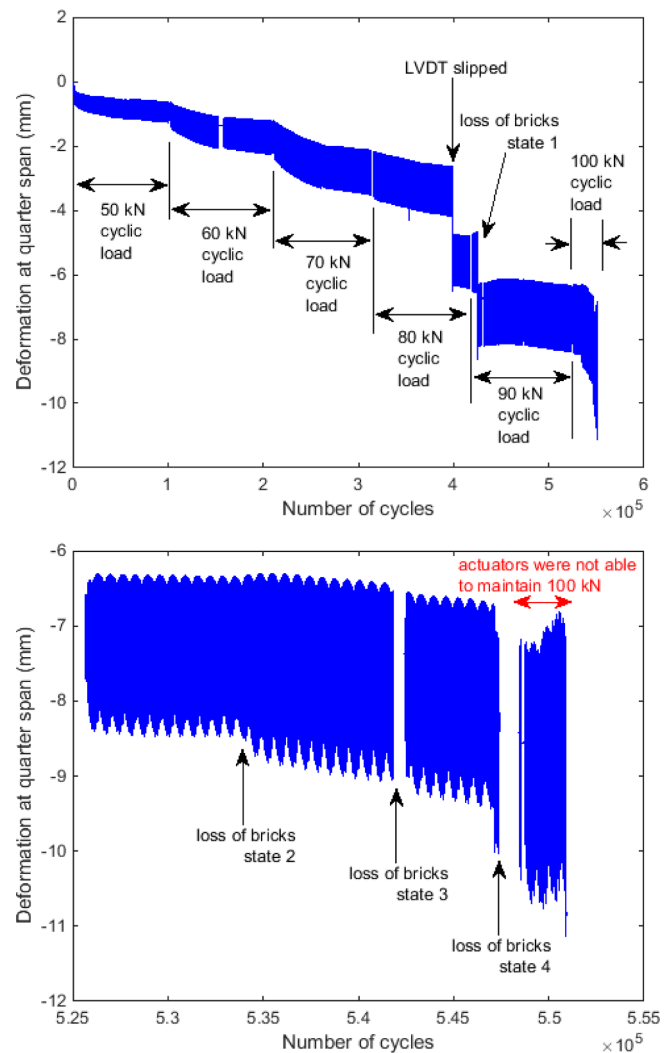


Fig. 9. EP5 – deformation at quarter span during faster cyclic loadings (a) from 50 kN to 100 kN (b) 100 kN.

The Design Manual of Roads and Bridges [13] suggests that a value of 50% of the ultimate load-carrying capacity may be considered as a ‘safe’ working load. For EP1 and EP2, the safe working load can be calculated as 70 kN (50% of failure load of 140 kN). Results of the 70 kN and 80 kN faster cyclic loading regimes (Fig. 9) show that the arch barrel does not show any significant distress and the deflection amplitudes were around 1.2 mm and 1.6 mm, respectively. This indicates that for the loading frequency of 2 Hz a 70 kN load complies with the DMRB guidance. During 80 kN faster cyclic loading, LVDT at quarter span slipped due to movement of bricks, as indicated by Fig. 9. Therefore, the loading frequency of 2 Hz a 80 kN load is more than the safe working load.

In addition, test results show that a 100 kN load at 2 Hz would demonstrably exceed the permissible and serviceability limit states due to significant deformation of the arch barrel. During the first EP1 quasi-static failure load test, the unload-reload loop (Fig. 5) indicates that the load of 90 kN does not alter the load–deflection path; both strength and stiffness appear to be unaffected. Therefore, it may be considered that the 90 kN load is within the elastic limit. However, during the dynamic load test of EP5, the 90 kN load level for cyclic loading at 2 Hz disturbed the arch barrel significantly. Therefore, frequency of the working load must be considered when defining the safe working load based on the permissible limits of a masonry arch bridge.

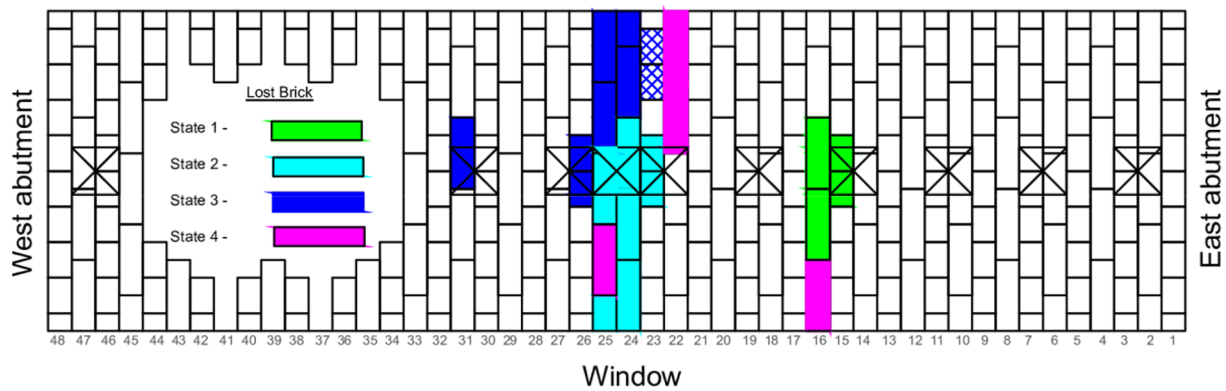


Fig. 10. Formation of fallen bricks during the cyclic loadings of EP5.



Fig. 11. Fallen intrados bricks near the crown of EP5 at the end of cyclic loadings.

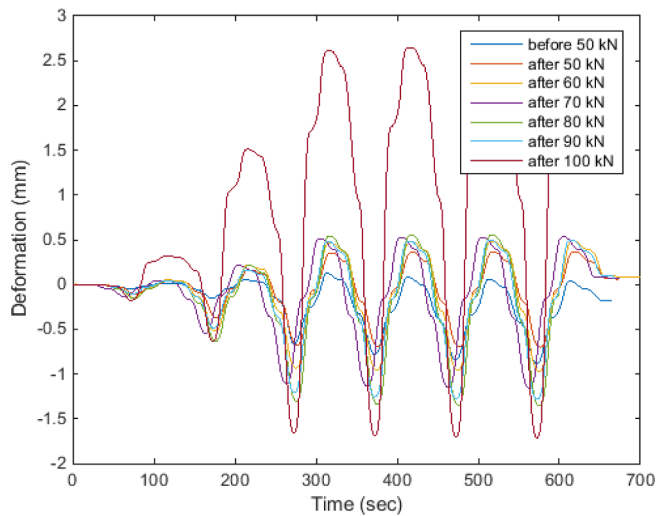


Fig. 12. Deformation amplitude during slower cyclic loading of EP5.

3.2. Damaged/distorted arch

In this section, any arch subjected to a 50 kN peak cyclic load at a loading frequency of 2 Hz was not considered as damaged or distorted. However, arches subjected to at least one failure load test or cyclic loading more than the permissible limit value was considered as damaged or distorted.

Table 3

Deformed profile of the arch barrel prior to quasi-static load tests. Positive and negative signs represent inward and outward directions, respectively. (all values in mm).

Test Phase	Radial deflection				
	West	3/4	1/2	1/4	East
EP1					
PH1-QS1-Start	0	0	0	0	0
PH2-QS2-Start	-5.26	-9.95	-1.56	9.52	-0.15
EP2					
PH1-QS1-Start	0	0	0	0	0
PH2-QS2-Start	-5.30	-28.49	-2.46	27.06	-0.37
EP4					
PH1-QS1-Start	0	0	0	0	0
PH2-QS2-Start	-23.90	-0.81	40.03	25.71	-0.67
PH3-QS3-Start	-30.48	-14.41	46.65	40.88	-1.34
EP5					
PH1-QS1-Start	-2.62	5.99	16.05	7.76	-3.98

3.2.1. Deformed shapes of arch bridges

Due to the different load tests applied to the different arches reported on, the level and form of distortion experienced by any given arch differs. The aim of this section is to consider the magnitude and form of deformation due to the quasi-static loading of a virgin arch. Table 3 presents the tabulated distorted shapes of EP1, EP2, EP4 and EP5 before all quasi-static load tests, allowing direct comparisons to be made. The distorted profiles are schematically illustrated in Fig. 13. It can be observed that the distorted shape before the second quasi-static load tests were influenced by the state when the first quasi-static load was released; in other words, the current state of the arch will influence the future behaviour of the arch. In the case of EP5, there were a series of cyclic loads applied to the arch at different stages, with only a single quasi-static load test to failure employed; hence the distorted shape of EP5 was only due to those cyclic loadings.

3.2.2. Damaged arch capacity

Fig. 14(a) presents applied load vs. deflection curves for the second quasi-static load test to failure of EP1 and EP2, where data is available. This data can be compared directly with that presented in Fig. 5, for the first quasi-static load test for EP1 and EP2, allowing observations to be made on the capacity of damaged arch structures. The data also allows an evaluation of the influence of the backfill material on both the initial capacity and also the damaged arch capacity as results are also presented for EP4.

The capacity as indicated in Fig. 14(a) can be seen to be reduced to

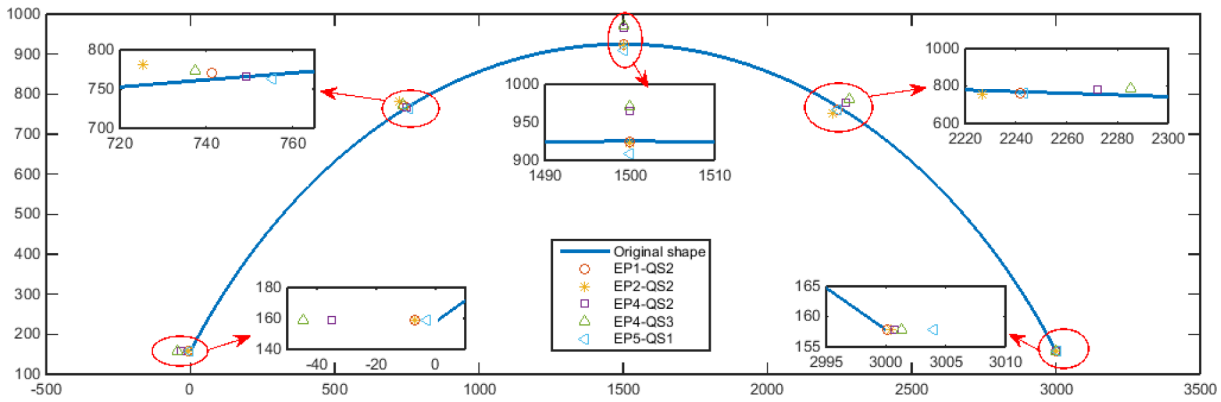


Fig. 13. Distorted shape of the arch barrel before each quasi-static failure load tests reported in this paper.

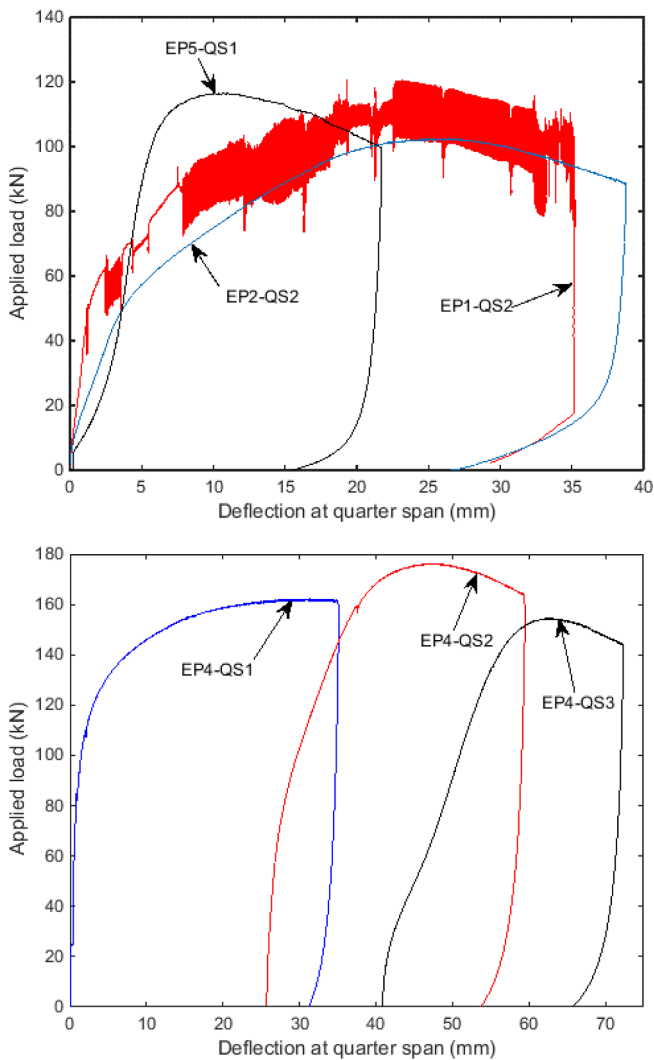


Fig. 14. (a) Second quasi-static load tests of EP1 and EP2, and first quasi-static load test of EP5 (b) All quasi-static load tests of EP4.

around 115 kN and 100 kN for EP1 and EP2, respectively. It is evident that the loss in capacity is more significant for EP2 than for EP1. Again, the difference between the two tests is the programme of cyclic loading (working loads) in EP1 that was absent in EP2, and the distorted shape at which the quasi-static (failure) load test was started (Table 3 and Fig. 13). In this case, the structural integrity of both arches had been compromised due to the first quasi-static load test.

The capacity of EP5 was around 115 kN, similar to EP1. It should be noted that the EP5 arch was subjected to various cyclic loading stages and a number of intrados bricks were dislocated completely prior to this quasi-static load test. In contrast to the second load test of EP1 and EP2, the EP5 test arch distorted significantly during the early stages of quasi-static loading.

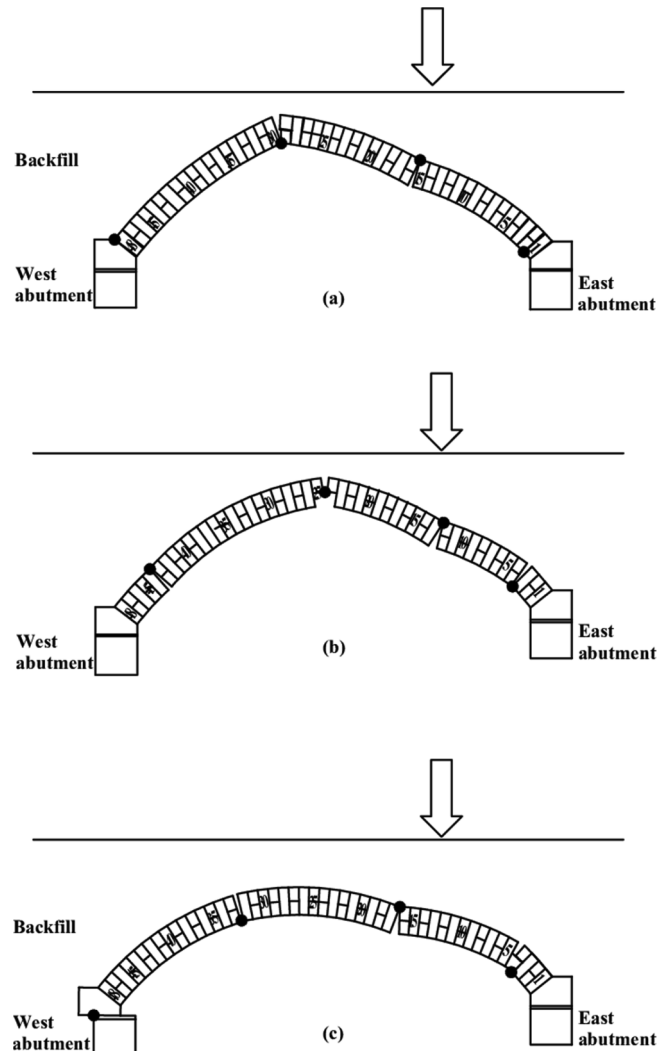


Fig. 15. Failure mechanism: (a) second quasi-static failure load test of EP1 and EP2; (b) first quasi-static failure load test of EP5; (c) second and third quasi-static failure load test of EP4.

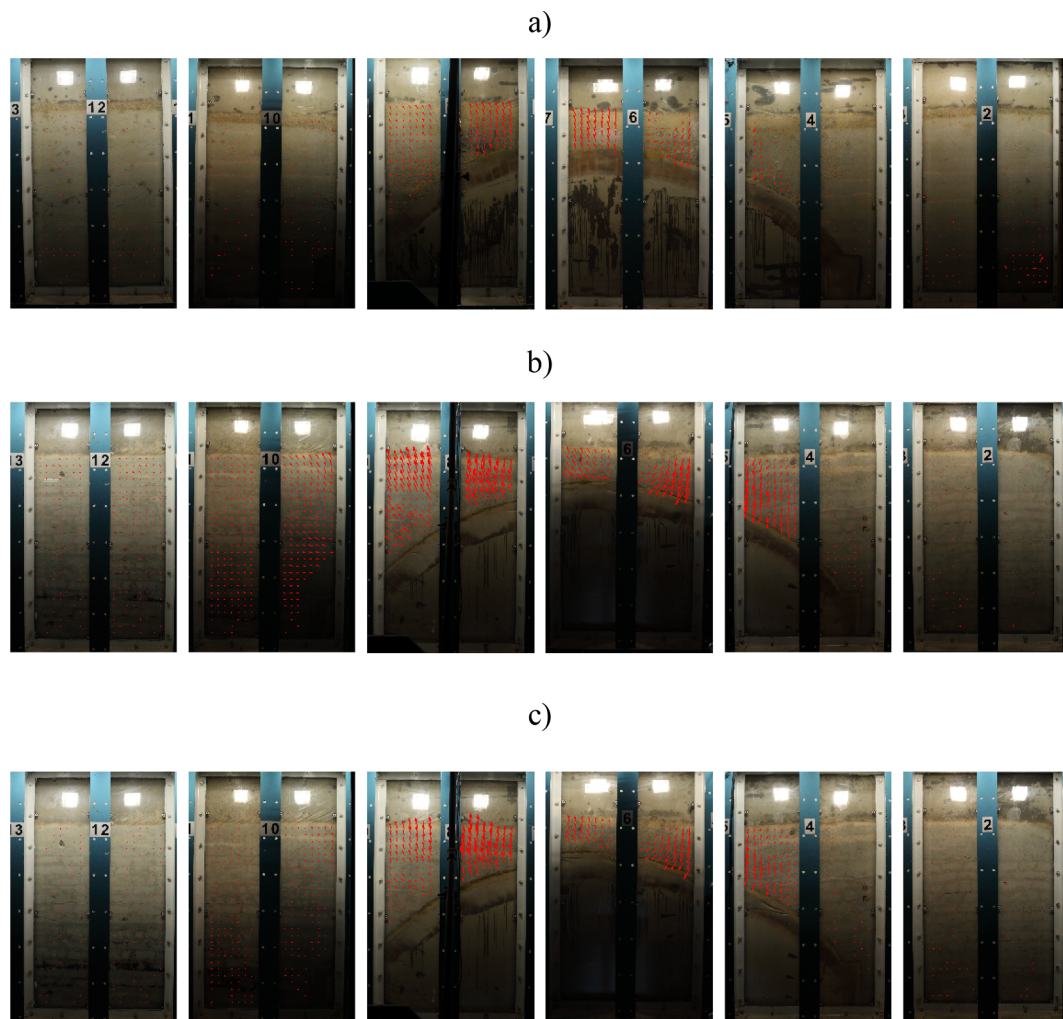


Fig. 16. Particle Image Velocimetry output from the start of the quasi-static test until maximum load carrying capacity of (a) EP5_QS1 (b) EP4_QS2 (c) EP4_QS3.

Failure mechanisms of the EP1 and EP2 test arches during the second quasi-static failure load tests were the same as observed during the first quasi-static load tests (Fig. 15(a)). This confirms that the locations of the hinges do not change unless the type of loading changes. The EP5 test arch was a four-hinge failure mechanism, however, the hinges were formed at different locations, as shown in Fig. 15(b). It should be noted that EP5 was subjected to various dynamic loading stages prior to quasi-static loading to failure and a hinge near the midspan was formed coincident with a loss of bricks, likely due to the dynamic loading. GeoPIV analysis of the second quasi-static load tests of EP1 and EP2 are not available. Image correlation analysis of EP5 confirms that the hinges were formed in the middle part of the arch (Fig. 16).

In the case of EP4, there were three quasi-static failure load tests undertaken. The first of these was reported earlier. However, for the purpose of comparison, all the failure load tests are compared in Fig. 14. At the point of release of applied load of the first quasi-static load test, the arch barrel exhibited three-hinges plus a sliding mechanism (Fig. 6(b)) as the clay backfill deformed as the abutment displaced. However, the second quasi-static failure test exhibited a four-hinge mechanism after initial sliding of the West abutment (Fig. 15(c)). For the third quasi-static load test, the arch barrel exhibited a four-hinge mechanism, where sliding at the west abutment was negligible, suggesting increased mobilisation of the clay backfill strength. As shown in Fig. 14, the second quasi-static load path meets the point where the first load was released and continues to carry slightly higher

loads, with a peak load slightly higher than the first peak load. The arch achieved an ultimate failure load of 170 kN with a four-hinge failure mechanism. The third quasi-static load test was performed on the damaged arch, and has a capacity of 150 kN. A similar percentage of load carrying capacity reduction was observed in EP1, EP2 and EP5. The evidences presented in this section suggests that damaged arches possess significant residual capacity. However, the residual capacity of the arch depends on the initial damaged or distorted condition of the arch barrel system.

3.2.3. Influence of cyclic loading on damaged/distorted arch bridges

In general, the stiffness of the system is expected to be lower for the arch barrel since in all cases they have been subjected to failure loads, and associated hinges, or changes in backfill strength and stiffness or structural damage due to excessive cyclic loading. The deflection amplitudes of slower cyclic loading tests before and after the quasi-static failure loads show that there was a significant change. This represents a change in the stiffness of the arch barrel due to the quasi-static failure load test, which could be used to justify the behaviour observed in the second failure load test.

EP4 was subjected to faster cyclic loading regimes with various peak loads after all three quasi-static load tests. The test results are shown in Fig. 17. As expected, deformation amplitude increased with increasing peak cyclic loadings. The arch barrel was intact for loads up to 78 kN, but, at 84 kN peak cyclic load, brick loss was observed, subsequently damaging the LVDT support frame (Figs. 17 and 18). Deformation

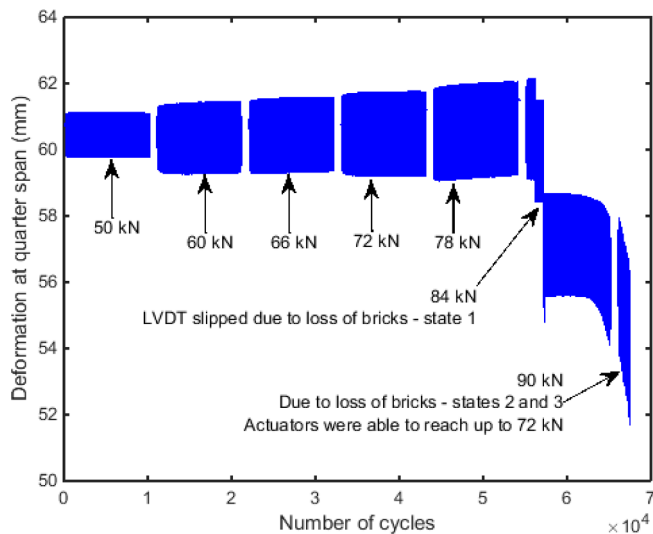


Fig. 17. Deformation amplitude during cyclic loadings of deformed bridges (after third quasi-static load test).

amplitude increased due to this incident. However, more significant disruption was observed when the peak cyclic load level reached 90 kN, and began soon after the start of this cyclic loading regime. A row of bricks near to the three-quarter span and a number of bricks near to the crown were lost (Figs. 17–19) and the load subsequently dropped to 72 kN. Due to the oil capacity of the hydraulic pump it was not possible to exceed a 90 kN peak cyclic load level.

The test results show that 50% of the ultimate load (maximum load taken by EP4 during third quasi-static load test was 150 kN) may be considered for the safe working load (i.e. 75 kN) based on the disturbance caused in the arch barrel alone, supported by visual observations during testing. Arch barrel deformations during the quasi-static load tests of EP1, EP2 and EP5 are summarised in Table 4, where the EP1 arch experienced a safe working load before the first and second quasi-static load tests, while the other two did not. Deformation during the second quasi-static load test of EP1 increased approximately three times compared to the first test. However, deformation increased more than six times during the second test of EP2 and the first test of EP5. The results suggest that the safe working loads applied to distorted and/or damaged arches significantly enhances the stiffness of the system and evidently ‘heals’ the arch to some extent. In addition, the magnitude of deflections observed at this current state may be within the allowable limits used by engineers. It should be noted that the distorted and damaged arches had permanent deformation from previous load tests, therefore the deflection may not meet the serviceability

limit criteria.

3.2.4. Safe working load of distorted/damaged arch

As mentioned before, most masonry arch bridges are more than one hundred years old. Over this time these structures have been subjected to various conditions: extreme loadings; deformation of abutments due to ground movements and scouring; deterioration of materials. Therefore, it is expected that the majority of masonry arch bridges are distorted and/or damaged to some degree. Identifying the serviceability or permissible limit states of the bridge based on the current state or condition is paramount for ensuring the continued resilience and longevity of these structures.

In the case of a virgin arch, as discussed earlier, a safe working load would be considered to be half of the ultimate load carrying capacity. This was confirmed based on the degree of disturbance to the brick arches during faster loading regimes. Table 4 compares the calculated safe load carrying capacity of EP1, EP2, EP4 and EP5 at different test stages and corresponding deflection amplitudes, where available. The deflection amplitudes are those taken toward the end of cyclic loading prior to determining the quasi-static failure load.

50 kN may be the safe working loads in accordance with the Highway Agency [13] guideline, however, deformations of distorted/damaged arch barrels were significantly higher than the virgin arch. This may be directly proportional to surface and near-surface deformation which in turn would significantly influences the comfort and safety of the passengers.

4. Conclusions

The paper reports on a series of laboratory tests on effectively full-scale backfilled masonry arch structures subjected to a wide range of loading conditions. The aim of the work presented was to explore the influence of loading history on arch behaviour and capacity, and more importantly, to examine the influence of loading history on the residual capacity of these important structures, an area that has to-date not been explored in detail, in spite of the clear importance and relevance to bridge owners and those charged with the task of assessing the engineering condition of these structures.

The application of safe working load levels, as defined in the Design Manual of Roads and Bridges [13] to define practical limits to the use of masonry arch structures (amongst other engineering structures) as part of a nation states infrastructure, to virgin backfilled masonry arch bridges tends to positively influence the behaviour of the arch system, due primarily to densification of the backfill soil, though this is likely to be influenced by the soil type and current soil state and condition; this is an area that needs much further investigation, as the type of soil backfill, its placement and changes to the material during the structure’s lifetime, is highly varied [24]. In this paper the authors have simplified this aspect to a coarse-grained material (crushed limestone)

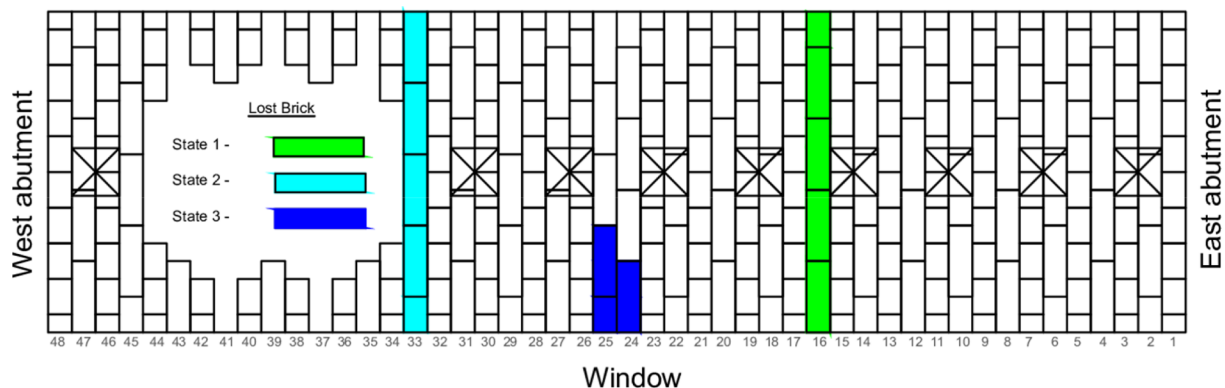


Fig. 18. Formation of fallen intrados bricks during the cyclic loadings of EP4.



Fig. 19. Pictures of fallen bricks after cyclic loading of deformed bridge of EP4.

Table 4

Deformation of arch barrel at quarter span applied load of 50 kN during quasi-static failure load tests.

Quasi-static failure load test	Deformation of arch barrel at applied load of 50 kN at quarter span (mm)
EP1-QS1	0.57
EP2-QS1	0.62
EP1-QS2	1.74
EP2-QS2	3.91
EP5-QS1	3.89

and fine-grained material (a generic clay). However, notwithstanding this issue, the general conclusion is broadly consistent; for virgin arches, the application of a safe working load provides a pragmatic approach to evaluating the likely behaviour of this form of infrastructure.

In addition, experimental data presented within this paper shows that the masonry arch barrels subjected to a 50 kN cyclic load over 10^6 cycles, broadly consistent with safe working load levels for the arches tested and reported on in this paper, show no observable damage to the structure, and importantly, the carrying capacity appears to be unaffected; there is a slight difference in the observed peak load level, analogous to the ULS, and the system stiffness is improved, although there is currently limited data on this latter aspect, which the authors believe is a key issue requiring appreciably more interest than currently documented in the wider literature.

For an arch-backfill system subjected to cyclic loading levels greater than the safe working load, as defined within the paper, much higher levels of structural disturbance are observed, which could lead to shorter life spans due to loss of masonry bricks, leading to earlier engineering intervention. Furthermore, the arch system may be unable to meet the deflection serviceability limit state. The presented data therefore emphasises the importance of identifying the safe working load level in ensuring masonry arch performance and longevity.

In addition, discussion of the data presented in this paper stresses the importance of the loading history of the masonry arch bridge as a significant factor which needs to be better understood by bridge owners and assessment engineers alike, as the arch system tends to hold a certain distorted shape even after the cessation of loading. However, when safe working load levels are applied to damaged arches, evidence of ‘healing’ is observed, and the structures can carry significant loads even when observed structural damage is significant.

Therefore, it is necessary to evaluate the current state of the masonry arch bridge. Evidence presented in this paper suggests that under some circumstances, a damaged masonry arch may still satisfy the ULS requirements, but not the serviceability requirements since deformations can be quite large. The permissible limit state (PLS; as defined by [17] might be a more appropriate measure of longer-term performance and capacity, although further experimental evidence is required to allow more confidence in applying the PLS.

Declaration of Competing Interest

The authors declare that they have no known competing financial interests or personal relationships that could have appeared to influence the work reported in this paper.

Acknowledgements

The authors wish to acknowledge the support of the UK Engineering and Physical Sciences Research Council (EPSRC) under grant references EP/I014357/1 and EP/I014489/1.

References

- [1] Acikgoz S, DeJong MJ, Soga K. Sensing dynamic displacements in masonry rail bridges using 2D digital image correlation. *Struct Control Health Monitor* 2018;25(8).
- [2] Augustus Nelson, L., Swift, G.M., Smith, C., Gilbert, M. and Melbourne, C., 2016. Behaviour of backfilled masonry arch bridges subjected to cyclic loading, 8th International Conference on Arch Bridges, October 5-7, 2016, Wrocław, Poland.
- [3] Augustus-Nelson L, Swift GM, Smith CC, Gilbert M, Melbourne C. Large-scale physical modelling of soil-filled masonry arch bridges. *Int J Phys Modell Geotech* 2018;18(2):81–94.
- [4] Augustus-Nelson L, Swift GM, Smith CC, Gilbert M, Melbourne C. Influence of railway loading on the performance of soil-filled masonry arch bridges. *Proc Inst Civ Eng – Bridge Eng* 2018;171(4):276–89. <https://doi.org/10.1680/jbren.17.00027>.
- [5] Boothby TE. Load rating of masonry arch bridges. *J Bridge Eng* 2001;6:79–86.
- [6] Callaway P, Gilbert M, Smith CC. Influence of backfill on the capacity of masonry arch bridges. *Proc Inst Civ Eng – Bridge Eng* 2012;165(3):147–57. <https://doi.org/10.1680/jbren.11.00038>.
- [7] Costa C, Ribeiro D, Jorge P, Silvac R, Arêde A, Calçada R. Calibration of the numerical model of a stone masonry railway bridge based on experimentally identified modal parameters. *Eng Struct* 2016;123:354–71.
- [8] Costa C, Arêde A, Morais M, Anfalc A. Detailed FE and DE modelling of stone masonry arch bridges for the assessment of load-carrying capacity. *Proc Eng* 2015;115:854–61.
- [9] De Santis S, de Felice G. Overview of railway masonry bridges with a safety factor estimate. *Int J Architect Herit* 2014;8:452–74.
- [10] Fanning, P.J. & Boothby, T.E. 2001. Three-dimensional modelling and full-scale testing of stone arch bridges. *Computers & Structures*, Issues 29–30, November 2001, 2645–2662.
- [11] Gilbert, M. 2001. Ring: a 2D rigid block analysis program for masonry arch bridges. In: *Proc. 3rd International arch bridges conference*, Paris, France: 109–118.
- [12] Gilbert, M., Melbourne, C., Smith, C., Augustus Nelson, L. and Swift, G.M., 2016. Proposed permissible limit state assessment criteria for masonry arch bridges. In *Proceedings of the 8th International Conference on Arch Bridges*, October 5-7, 2016, Wrocław, Poland.
- [13] Highway structures: Design (substructures and special structures), materials. Special structures. Unreinforced masonry arch bridges. 2004 DMRB Volume 2 Section 2 Part 14 (BD 91/04), Highways Agency, The Stationery Office, London.
- [14] Hughes, T. G. & Blackler, M. J. 1997. A review of the UK masonry arch assessment methods. *Proceedings of the Institution of Civil Engineers – Structures and Buildings*. 122(3): 305–315.
- [15] Martin-Caro JA. *Puentes de Fabrica. Los puentes ferroviarios dentro del patrimonio industrial* [Fabrica bridges. The railway bridges within the industrial heritage]. Madrid: ADIF; 2013.
- [16] Melbourne, C., & Alnuaimi, M. M. 2001. The behaviour of multi-ring brickwork arches subjected to cyclic loading. In *Proceedings of the 3rd International Arch Bridge Conference*, Paris.
- [17] Melbourne, C., Wang, J. & Tomor, A. 2007. A new masonry arch bridge assessment

- method (SMART) Proceeding of the Institution of Civil Engineers, Bridge Engineering. 160(2): 81–87.
- [18] Melbourne, C., Cole, G., Gilbert, M., Swift, G. & Smith, C. 2013. A road-map for the assessment of masonry arch bridges. In Proceedings of the 7th International Arch Bridges Conference, Croatia, 605-612.
- [19] McKibbins, D.L., Melbourne, C., Sawar, N., Gaillard, S. C. 2006. Masonry arch bridges: Condition appraisal and remedial treatment. Report C656, CIRIA, London.
- [20] Milani C, Lourenço PB. 3D non-linear behavior of masonry arch bridges. *Comput Struct* 2012;110–111:133–50.
- [21] Orbán Z. UIC project on assessment, inspection and maintenance of masonry arch railway bridges. *ARCH* 2007;7:3–12.
- [22] Orbán Z, Gutermann M. Assessment of masonry arch railway bridges using non-destructive in-situ testing methods. *Eng Struct* 2009;31:2287–98.
- [23] Page, J., Ives, D. A. and Ashurst, D. 1991. Deterioration and repair of masonry arch bridges. In Proceedings of the 9th International Brick/Block Masonry Conference, DGfM, ed., Berlin, 1591–1599.
- [24] Smith, C.C., Gilbert, M. and Callaway, P.A. 2004. Geotechnical issues in the analysis of masonry arch bridges. Proceedings of the 4th International Arch Bridges Conference, Barcelona, Spain, 343–352.
- [25] Swift, G. M., Augustus-Nelson, L., Melbourne, C. & Gilbert, M. 2013. Physical modelling of cyclically loaded masonry arch bridges. In Proceedings of the 7th International Arch Bridges Conference, Croatia, 621–628.
- [26] CS 454, The Assessment of Highway Bridges and Structures (formerly, BD21/01). Design Manual for Roads and Bridges, Volume 3, Section 4, Part 3., 2019, Highways England, UK.
- [27] Yea C, Acikgoz S, Pendrigha B, Riley E, DeJong MJ. Mapping deformations and inferring movements of masonry arch bridges using point cloud data. *Eng Struct* 2018;173:530–45.